

## Supporting Information

# Thermodynamics of Hydrogen Adsorption in Slit-Like Carbon Nanopores at 77 K. Classical Versus Path Integral Monte Carlo Simulations

Piotr Kowalczyk<sup>a,c\*</sup>, Piotr A. Gauden<sup>b</sup>, Artur P. Terzyk<sup>b</sup>, Suresh K. Bhatia<sup>c</sup>

<sup>a</sup>Department III, Soft condensed matter  
Institute of Physical Chemistry of the Polish Academy of Sciences

<sup>b</sup>Physicochemistry of Carbon Materials Research Group, Faculty of Chemistry,  
Nicolaus Copernicus University, 7 Gagarina Str., 87-100 Toruń, Poland

<sup>c</sup>Division of Chemical Engineering, The University of Queensland,  
St. Lucia, Qld 4072, Australia

### **Langmuir**

Number of pages: 16

Number of figures: 5

Number of movies: 5

## Simulation details

### a. Potential Models

Following the Feynman's path integral formalism we used the quantum-classical isomorphism: in which each particle becomes equivalent to a chain or "necklace" of  $P$  classical "beads"  $\mathbf{r}_1^{(j)}$ ,  $\mathbf{r}_2^{(j)}$ ,  $\mathbf{r}_3^{(j)}$ , ...,  $\mathbf{r}_P^{(j)}$  that account for the quantum dispersion of the particle<sup>1-3</sup>. In other words, each quantum particle maps onto a ring polymer held together by Hooke's law springs<sup>4</sup>. The configuration space spanned by the  $P$  classical particles is the space spanned by a quantum particle obeying the uncertainty principle. As the mass or temperature of the particle increases, the uncertainty diminishes; the space is the same as that spanned by one classical particle. The path integral formalism is exact for the Trotter number  $P \rightarrow \infty$ <sup>1-4</sup>. Clearly, in the classical limit that is for  $P = 1$ , all quantum fluctuations are ignored (*i.e.* in the classical limit all the points on the polymer or necklace coalesce to a single point in space). The variance of the entire polymer or necklace is  $\beta\hbar^2/m$  ( $\beta^{-1} = k_B T$ ,  $\hbar = h/2\pi$ ,  $m$  is the mass of the quantum molecule,  $h$  denotes Planck's constant,  $k_B$  denoted Boltzmann's constant)<sup>1</sup>. This picture is illustrated in Figure 1S.

In a bulk quantum fluid ring polymers experience both an external potential, due to other molecules in the fluid, and internal potential, which comes from the intermolecular bonding interactions. The effective potential can be expressed according to the so-called "primitive propagator"<sup>5-10</sup>,

$$W_{\text{ff}} = \frac{mP}{2\beta^2\hbar^2} \sum_{i=1}^N \sum_{\alpha=1}^P (\mathbf{r}_i^{(\alpha)} - \mathbf{r}_i^{(\alpha+1)})^2 + \frac{1}{P} \sum_{i < j} \sum_{\alpha=1}^P V_{\text{ff}}(\mathbf{r}_{ij}^{(\alpha)}) \quad (1)$$

Notice that the primed  $\alpha$  summation in the above equation is cyclic; that is to say, if  $\alpha = P$ , then  $\alpha + 1 = 1$ .

In the infinitely long structureless slit-like carbon pore the primitive propagator is additionally supplemented by the term resulting from the external interaction between the ring polymer and graphite solid surfaces comprising the pore walls (*c.f.* Figure 1)<sup>11-13</sup>,

$$W_{\text{P}} = W_{\text{ff}} + \frac{1}{P} \sum_{i=1}^N \sum_{\alpha=1}^P V_{\text{sf}}(\mathbf{z}_i^{(\alpha)}) \quad (2)$$

Similar to Tanaka *et al.*<sup>14,15</sup>, Levesque *et al.*<sup>16</sup>, Kumar *et al.*<sup>17,18</sup>, and Kowalczyk *et al.*<sup>19</sup> we modeled the external interactions between the beads of the ring polymers via the effective truncated one-centre Lennard-Jones potential (*i.e.* we treated the hydrogen as a quasi-spherical molecule),

$$V_{\text{ff}}(\mathbf{r}_{ij}^{(\alpha)}) = 4\varepsilon_{\text{ff}} \left[ \left( \frac{\sigma_{\text{ff}}}{\mathbf{r}_{ij}^{(\alpha)}} \right)^{12} - \left( \frac{\sigma_{\text{ff}}}{\mathbf{r}_{ij}^{(\alpha)}} \right)^6 \right] \Theta(\mathbf{r}_{ij}^{\text{cut}} - \mathbf{r}_{ij}^{(\alpha)}) \quad (3)$$

Here,  $\mathbf{r}_{ij}^{(\alpha)}$  is the distance between the beads labeled  $\alpha$  of two interacting ring polymers,  $\sigma_{\text{ff}}$  denoted Lennard-Jones collision diameter,  $\varepsilon_{\text{ff}}$  is the Lennard-Jones well-depth,  $\mathbf{r}_{ij}^{\text{cut}} = 5\sigma_{\text{ff}}$  is the cutoff distance, and  $\Theta$  denotes Heaviside function. The Lennard-Jones parameters for hydrogen interactions,  $\sigma_{\text{ff}} = 2.958 \text{ \AA}$  and  $\varepsilon_{\text{ff}} / k_{\text{B}} = 36.7 \text{ K}$ , were taken from previous studies<sup>15-19</sup>.

The external potential between an individual bead of the ring polymer and carbon surfaces is a sum of those generated from infinite planes comprising the walls of the slit-like pore (*c.f.* Figure 1S)<sup>20</sup>,

$$V_{\text{sf}}(\mathbf{z}_i^{(\alpha)}) = \sum_{j=0}^{M-1} V_{10-4}(H - \mathbf{z}_i^{(\alpha)} + j \cdot \Delta) + \sum_{j=0}^{M-1} V_{10-4}(\mathbf{z}_i^{(\alpha)} + j \cdot \Delta) \quad (4)$$

Here  $M - 1$  denotes the number of graphite planes comprising the pore wall (here  $M = 4$ ) and  $H$  denotes slit width (*c.f.* Figure 1S). The distance between graphitic planes is taken as that for graphite ( $\Delta = 3.35 \text{ \AA}$ )<sup>21</sup>. The potential between a hydrogen molecule and a single infinite plane of structureless graphite is modeled by the Steele 10-4 potential<sup>20,21</sup>,

$$V_{10-4}(\mathbf{z}_i^{(\alpha)}) = 4\varepsilon_{\text{sf}} \pi \rho_s \sigma_{\text{sf}}^2 \left[ \frac{1}{5} \left( \frac{\sigma_{\text{sf}}}{\mathbf{z}_i^{(\alpha)}} \right)^{10} - \frac{1}{2} \left( \frac{\sigma_{\text{sf}}}{\mathbf{z}_i^{(\alpha)}} \right)^4 \right] \quad (5)$$

where  $\rho_s = 38.2 \text{ nm}^{-2}$  is the surface density of carbon atoms<sup>20</sup>,  $\sigma_{\text{sf}}$  and  $\varepsilon_{\text{sf}}$  denotes Lennard-Jones solid-fluid collision diameter and well-depth, respectively, and  $\mathbf{z}_i^{(\alpha)}$  is the distance of

the bead labeled  $\alpha$  of the individual ring polymer from the plane. The parameters of the solid-fluid potential were calculated from the Lorentz-Berthelot mixing rule. For carbon we adapted the following values of parameters  $\sigma_{ss} = 3.4 \text{ \AA}$  and  $\varepsilon_{ss} / k_B = 28 \text{ K}^{20,21}$ .

Due to the uncertainty principle the structure of the (discretized) quantum model is richer than that of its classical counterpart. The primary quantity describing the quantum spreading is the gyration radius of the ring polymer<sup>1-10</sup>,

$$\langle R_g \rangle = \left\langle \frac{1}{P} \sum_{\alpha=1}^P |\mathbf{r}_i^{(\alpha)} - \mathbf{R}_{i,\text{cm}}| \right\rangle \quad (6)$$

where  $\mathbf{R}_{i,\text{cm}}$  stands for the coordinates of the  $i$ -necklace "centre of mass", and  $\langle \dots \rangle$  is the ensemble average computed from Monte Carlo simulations. As in the classical theory of polymers the average gyration radius is an effective quantity that characterizes the size of the polymer. However, for the case of the quantum mechanics according to Feynman's path integral theory such quantity is responsible for the wave nature of light particles<sup>1-3</sup>.

## b. Path Integral Monte Carlo Simulation in the Canonical Ensemble

For the investigation of quantum effects in bulk hydrogen at 77 K and pressures up to 4 MPa we used path integral Monte Carlo simulation in the canonical ensemble (*i.e.*, fixed system volume  $V$ , temperature  $T$ , and the number of molecules  $N$ )<sup>22,23</sup>. A cubic simulation box of size  $M\sigma_{\text{ff}} \cdot M\sigma_{\text{ff}} \cdot M\sigma_{\text{ff}}$ ,  $M \geq 10$  with periodic boundary conditions in all directions was used, with the minimum image convention used for computation of molecular interactions<sup>22,23</sup>. For the very low density region bulk hydrogen fluid obeys the ideal gas law. In this region we adjusted  $M$  following with the condition that at least 50 hydrogen molecules are in the simulation box. For higher pressures, we used the same adjustment procedure with the condition that at least 100 hydrogen molecules are in the simulation box. The number of beads per ring polymer was adjusted by comparison of the computed equation of state with the experimental one<sup>24</sup>. Additionally, we monitored the variation of the average gyration radius of the cyclic polymer versus the number of the beads per ring polymer. We find that the number of the beads equal 12 per ring polymer captures quantum dispersion of the hydrogen at 77 K and moderate pressures. The bead-bead intermolecular cutoff distance was set to  $5\sigma_{\text{ff}}$ . The initial configurations were generated by assessing the positions of the

centers of ring polymers forming on fcc lattice<sup>22,23</sup>. Next all beads were randomly created according to a gaussian normal distribution with small variance. Additionally, we assigned the initial position of the ring polymer centre from the final equilibrium positions obtained from classical Monte Carlo simulation. We did not find significant influence of the initial configuration of the paths on the final statistical averages computed from Monte Carlo method in the canonical ensemble.

The single displacement step was accepted according to standard Metropolis sampling scheme<sup>22,23</sup>,

$$acc(s \rightarrow s') = \min\{1, \exp(-\beta\Delta W_{\text{ff}})\} \quad (7)$$

where  $\Delta W_{\text{ff}} = W_{\text{ff}}(\mathbf{r}'^N) - W_{\text{ff}}(\mathbf{r}^N)$  is the change in the total energy (*i.e.* the path integral Hamiltonian). In our computational software we performed two-steps displacement perturbation of a randomly selected ring polymer. At first, we randomly moved the centre of the selected cyclic path. Subsequently, we randomly moved the selected bead of the displaced ring polymer. Displacement step size has been adjusted to give acceptance ratio of 50 %.

We calculated the excess part of the chemical potential of hydrogen in the canonical ensemble according to Widom's test particle insertion method and the corresponding bulk pressure of hydrogen from the virial theorem<sup>22,23,25</sup>. We developed a simple algorithm for insertion of the ghost ring polymer into bulk hydrogen fluid at equilibrium. At first, we randomly swapped the one hydrogen polymer ring and tabulated the distances between the centre of the cyclic path and all its beads. Following that, we inserted the trial centre of the ghost cyclic path into the fluid at a random location. Finally, all beads are inserted with random orientation at the distances tabulated before. Notice that in the proposed algorithm we inserted the test ghost cyclic path at random position and orientation, considering the average gyration radius of the swapped hydrogen molecule at equilibrium. Following Wang *et al.*<sup>26</sup> only the intermolecular interaction was used in the calculation of the test particle insertion energy. In the canonical ensemble  $2.6 \cdot 10^8$  configurations were generated. We discarded the first  $2 \cdot 10^8$  configurations to guarantee equilibration, whereas the latter  $6 \cdot 10^7$  configurations were used to obtain the desired thermodynamic properties.

### c. Path Integral Monte Carlo Simulation in Grand Canonical Ensemble

In the simulation of hydrogen adsorption in the idealized slit-like carbon nanopores we used a grand canonical ensemble (*i.e.*, fixed system volume  $V$ , temperature  $T$ , and the chemical potential of the bulk fluid  $\mu_p$ )<sup>23,24,26</sup>. We adopted free types of moves in our path integral GCMC simulations: particle displacement, particle creation, and particle deletion. The probability of accepting a trial displacement move is given by Eq. 7.

The trial insertion/deletion of particle was performed according to Wang and Johnson<sup>26-28</sup> description. In the molecule creation steps a ring polymer is inserted in the simulation box with a random position and orientation. For this purpose we randomly selected the centre of the inserted path. Following that we inserted the ring polymer with conformation picked from the configurations of the ideal gas polymer system. Clearly, conformations of ideal gas ring polymer system were generated in canonical ensemble at the same external conditions. Following to Wang and Johnson the probability of particle insertion consist only with external interactions of inserted path with all remaining  $N$  ones<sup>26-28</sup>,

$$acc(N \rightarrow N + 1) = \min \left\{ 1, \frac{V}{(N + 1)\Lambda^3} \exp \langle \beta (\mu_p - w_\Gamma^{\text{ext}}) \rangle \right\} \quad (8)$$

where  $\mu_p$  denote chemical potential,  $V$  is the volume of the simulation box,  $\Lambda = \sqrt{h^2 / (2\pi mkT)}$  is the de Broglie wavelength,  $w_\Gamma^{\text{ext}}$  is the interaction of the inserted ring polymer with all remaining ones in the fluid and solid surface, and  $\Gamma$  denotes the conformation of the particle inserted into simulation box.

Similarly, the removal of particle is accepted with a probability<sup>26-28</sup>,

$$acc(N \rightarrow N - 1) = \min \left\{ 1, \frac{\Lambda^3 N}{V} \exp \langle \beta (w_\Gamma^{\text{ext}} - \mu_p) \rangle \right\} \quad (9)$$

where  $w_\Gamma^{\text{ext}}$  is the interaction of the deleted ring polymer with the remaining  $N - 1$  ones in the fluid and solid surface, and  $\Gamma$  denotes the conformation of the deleted from the simulation box. Please note that as for particle insertion only external interactions appears in the acceptance probability for particle deletion.

To maintain microscopic reversibility we set up equal probability for trial displacement, creation, and destruction of selected particle. Both the pressure and chemical potential of hydrogen calculated in canonical ensemble were used as an input in path integral GCMC simulations. As in canonical ensemble the bead-bead intermolecular cutoff distance was set to  $5\sigma_{\text{ff}}$ . To trace the isotherms, we mimic experimental procedures by starting with an empty simulation box. Simulation runs were performed at gradually increasing chemical potentials, and the resulting configurations of one condition were used to initiate the subsequent calculations at higher chemical potentials. The grand canonical ensemble simulations utilized  $2 \cdot 10^8$  configurations, of which the first  $1 \cdot 10^8$  were discarded to guarantee equilibration. The stability of the results was confirmed by additional longer runs of  $1 \cdot 10^8$  configurations, with the equilibrium averages for hydrogen in pores fully reproducible.

#### **d. Classical Molecular Dynamics**

We used classical  $(N, V, T)$  molecular dynamics simulations (MD) to confirm the range of deviations of the computed hydrogen EOS for experimental data at 77 K and pressures up to 4 MPa<sup>23,24</sup>. The MD simulations were performed for a system containing of at least 1000 hydrogen molecules interacting via Eq. 3. We adopted a large simulation box of size  $20\sigma_{\text{ff}} \cdot 20\sigma_{\text{ff}} \cdot 20\sigma_{\text{ff}}$  surrounded by periodic boundary conditions in all directions. The intermolecular cutoff distance was set to  $10\sigma_{\text{ff}}$ . The initial configurations were generated by assessing the positions of hydrogen molecules from an fcc lattice<sup>23,24</sup>. For the integration of intermolecular forces corresponding to Eq.3 we used the Verlet algorithm with reduced time step  $\Delta\tau^* = \Delta\tau(m\sigma_{\text{ff}}^2 / \epsilon_{\text{ff}}) = 0.001$  (*i.e.* 0.76 fs)<sup>23,24</sup>. To maintain the desired temperature and thermodynamic equilibrium the system was equilibrated during 1.1 ns. We used standard algorithm for rescaling of molecular velocity for temperature adjustment<sup>23,24</sup>. After the equilibration we collected the hydrogen equation of state during next 0.46 ns. The pressure was computed from virial theorem<sup>23,24</sup>.

#### **e. Thermodynamics of Hydrogen Adsorption**

Path Integral GCMC and classical GCMC simulation allows for a precise determination of the total uptake of hydrogen in pore at thermodynamic equilibrium because

the geometry of the adsorbent is specified<sup>29,30</sup>. Based on the absolute value of adsorption the total stored volumetric energy was calculated following the expression<sup>19</sup>,

$$\Omega = \Gamma_{\text{H}} \cdot (-\Delta H_{\text{H}}) \quad (10)$$

Here,  $\Delta H_{\text{H}}$  denotes the heat of hydrogen combustion respectively. Following Dell and Rand the heat of combustion of hydrogen equates to the heat of formation of the product water, *i.e.*  $-285.83$  kJ per mol water ( $-141.789$  MJ per kg hydrogen)<sup>31</sup>.

During adsorption the heat is released since this process is exothermic. The amount of the released heat is closely related to the specific adsorbate-adsorbent and adsorbate-adsorbate interactions. Moreover, the heat production during adsorption is more sensitive to the heterogeneity of the material than the standard adsorption isotherm measurements. Fluctuation theory allows calculation of the isosteric enthalpy of adsorption from PIGCMC simulation<sup>23</sup>,

$$q_{st} = \frac{5}{2} k_{\text{B}} T - \frac{\langle EN \rangle - \langle E \rangle \langle N \rangle}{\langle N^2 \rangle - \langle N \rangle^2} \quad (11)$$

For the “primitive propagator” we can write the equation for the total energy as follows<sup>7-10</sup>,

$$E = \frac{3}{2} NP k_{\text{B}} T - W_1 + W_2 \quad (12)$$

where  $N$  denotes the number of particles, and the  $W_i$ ,  $i = 1, 2$  coefficients are given by<sup>7-10</sup>,

$$W_1 = \frac{mP}{2\beta^2 \hbar^2} \sum_{i=1}^N \sum_{\alpha=1}^P (\mathbf{r}_i^{(\alpha)} - \mathbf{r}_i^{(\alpha+1)})^2 \quad (13)$$

$$W_2 = \frac{1}{P} \left[ \sum_{i < j} \sum_{\alpha=1}^P V_{\text{ff}}(\mathbf{r}_{ij}^{(\alpha)}) + \sum_{i=1}^N \sum_{\alpha=1}^P V_{\text{sf}}(\mathbf{z}_i^{(\alpha)}) \right] \quad (14)$$

Combining Eq. 11 and 12 yield,

$$q_{\text{st}} = \frac{5}{2}k_{\text{B}}T - \frac{3}{2}Pk_{\text{B}}T - \frac{\langle W_2 N \rangle - \langle W_2 \rangle \langle N \rangle}{\langle N^2 \rangle - \langle N \rangle^2} - \frac{\langle W_1 \rangle \langle N \rangle - \langle W_1 N \rangle}{\langle N^2 \rangle - \langle N \rangle^2} \quad (15)$$

In the above equation  $\langle \dots \rangle$  is the ensemble average calculated from PIGCMC simulation. Obviously, due to quantum fluctuations Eq. 15 contains correction to the classical kinetic energy, which is known as Barker or thermodynamics estimator<sup>32</sup>,

$$K_{\text{B}} = \frac{3}{2}Nk_{\text{B}}TP - \frac{mP}{2\beta^2\hbar^2} \sum_{i=1}^N \sum_{\alpha=1}^P (\mathbf{r}_i^{(\alpha)} - \mathbf{r}_i^{(\alpha+1)})^2 \quad (16)$$

In classical limit that is for  $P = 1$  Eq 15 can be rewritten as follows<sup>23</sup>,

$$q_{\text{st}} = k_{\text{B}}T - \frac{\langle W_2 N \rangle - \langle W_2 \rangle \langle N \rangle}{\langle N^2 \rangle - \langle N \rangle^2} \quad (17)$$

Note that for  $P = 1$  the term accounting for the necklace bead harmonic couplings vanishes, and the kinetic energy is equal to  $(3/2)k_{\text{B}}T$ . That is why Eq. 17 reduces to the well-known formula describing the isosteric enthalpy of adsorption of classical fluids.

## References

- (1) Chandler, D. in Hansen, J.P.; Levesque, D.; Zinn-Justin, J., eds. *Theory of Quantum Processes in Liquids*; Elsevier: Amsterdam, 1991.
- (2) Feynman, R.P. *Statistical Mechanics*; Benjamin: New York, 1972.
- (3) Feynman, R.P.; Hibbs, A. *Quantum Mechanics and Path Integrals*; McGraw-Hill: New York, 1965.
- (4) Binder, K.; Heermann, D.W. *Monte Carlo Simulation in Statistical Physics*; Springer-Verlag: Berlin, 2002.
- (5) Wang, Q.; Johnson, J.K. *J. Chem. Phys.* **1999**, 110, 577.
- (6) Wang, Q.; Johnson, J.K. *J. Phys. Chem. B* **1999**, 103, 277.
- (7) Sese, L. M. *Mol. Phys.* **1994**, 81, 1297.
- (8) Sese, L. M. *Mol. Phys.* **1995**, 85, 931.
- (9) Sese, L. M. *Chem. Phys. Lett.* **1997**, 266, 130.
- (10) Sese, L. M. *Mol. Phys.* **1993**, 78, 1167.
- (11) Wang, Q.; Challa, S.R.; Sholl, D.S.; Johnson, J.K. *Phys. Rev. Lett.* **1999**, 82, 956.
- (12) Challa, S.R.; Scholl, D.S.; Johnson, J.K. *Phys. Rev. B* **2001**, 63, 245419.
- (13) Challa, S.R.; Scholl, D.S.; Johnson, J.K. *J. Chem. Phys.* **2002**, 116, 814.
- (14) Tanaka, H.; Kanoh, H.; Yudasaka, M.; Iijima, S.; Kaneko, K. *J. Am. Chem. Soc.* **2005**, 127, 7511.
- (15) Tanaka, H.; Fan, J.; Kanoh, H.; Yudasaka, Yudasaka.; Iijima, S.; Kaneko, K. *Mol. Simul.* **2005**, 31, 465.
- (16) Levesque, D.; Gicquel, A.; Darkrim, F. L.; Kayiran, S. B. *J. Phys. Con. Matt.* **2002**, 14, 9285.
- (17) Kumar, A.V.A.; Bhatia, S.K. *Phys. Rev. Lett.* **2005**, 95, 245901.
- (18) Kumar, A.V.A.; Jobic, H.; Bhatia, S.K. *J. Phys. Chem. B* **2006**, 110, 16666.
- (19) Kowalczyk, P.; Holyst, R.; Terzyk, A.P.; Gauden, P.A. *Langmuir* **2006**, 22, 1970.
- (20) Steele, W. A. *The Interaction of Gases with Solid Surfaces*; Pergamon Press: Oxford, 1974.
- (21) Do, D. D. *Adsorption Analysis: Equilibria and Kinetics*; Imperial College Press, London, 1998.
- (22) Frenkel, D.; Smit, B. *Understanding Molecular Simulation From Algorithms To Applications*; Academic Press: London, 1996.
- (23) Allen, M.P.; Tildesley, D.J. *Computer Simulation of Liquids*; Clarendon: Oxford, 1987.

- (24) Vagraftik, N.B. *The Handbook of Thermodynamic Properties of Gases and Liquids*; G.I.F.M.L., Moscow, 1963 (in Russia).
- (25) Widom, B. *J. Chem. Phys.* **1963**, 39, 2808.
- (26) Wang, Q.; Johnson, K.J.; Broughton, J.Q. *Mol. Phys.* **1996**, 89, 1105.
- (27) Wang, Q.; Johnson, J.K. *Fluid Phase Equilibria* **1997**, 132, 93.
- (28) Wang, Q.; Johnson, J.K.; Broughton, J.Q. *J. Chem. Phys.* **1997**, 107, 5108.
- (29) Nicholson, D.; Parsonage, N. G. *Computer Simulation and the Statistical Mechanics of Adsorption*; Academic Press: London, 1982.
- (30) Rzepka, M; Lamp, P.; de la Casa-Lillo, M. A. *J. Phys. Chem. B* **1998**, 102, 10894.
- (31) Dell, R.M.; Rand, D.A.J *Clean Energy*; The Royal Society of Chemistry, Cambridge: 2004.
- (32) Barker, J.A. *J. Chem. Phys.* **1979**, 70, 2914.
- (33) Silvera, I.F.; Goldman, V.V. *J. Chem. Phys.* **1978**, 69, 4209.

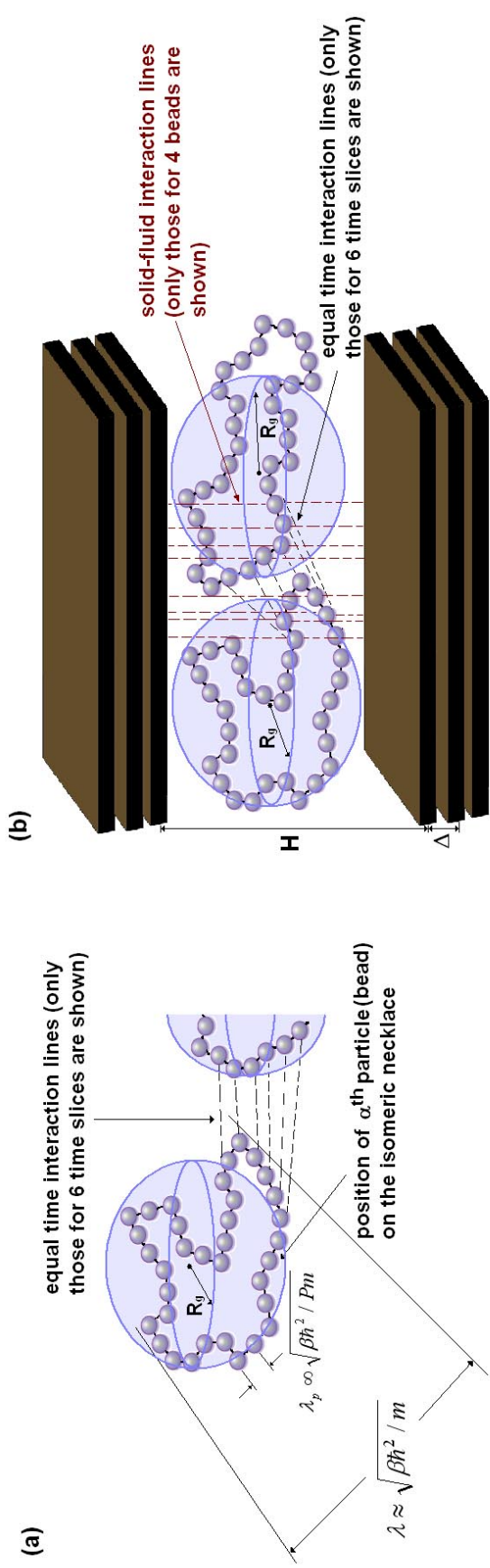


**Figure 1S.** Panel (a) - schematic representation of the path integral necklace quantizing two particles. The length  $\lambda \approx \hbar^2 / \langle (\Delta p)^2 \rangle \approx \sqrt{\beta \hbar^2 / m}$  is the uncertainty spreading or thermal wavelength for a particle of mass  $m$ . The distance between effective monomers in the ring polymer scales as  $\lambda_p \propto \sqrt{\beta \hbar^2 / Pm}$  (integer  $P$  is the Trotter number) denotes the same quantity between two neighbour isomeric necklaces,  $R_g$  denotes the radius of gyration of ring polymer. Panel (b) – schematic representation of the path integral necklace quantizing two molecules confined in the infinitely long structureless slit-like carbon pore,  $H$  is the pore width, and  $\Delta$  denotes interlayer distance between the graphite planes composing the pore wall.

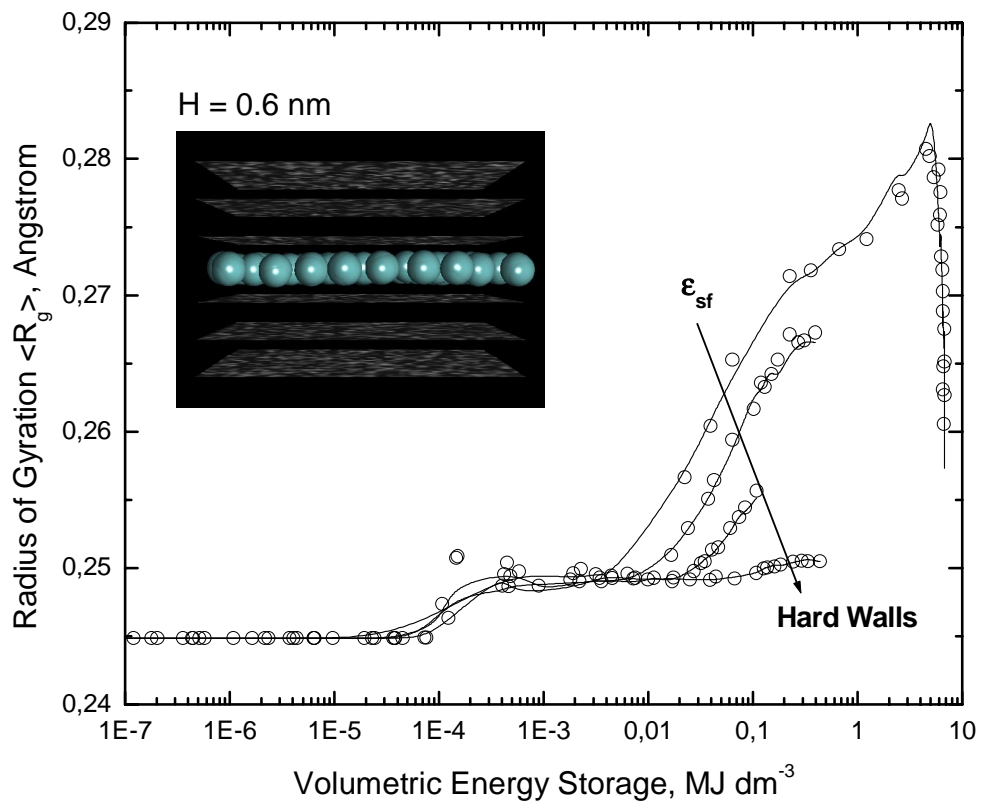


**Figure 2S.** Impact of the strength of  $\epsilon_{sf}$  on the average size of adsorbed hydrogen ring polymers in slit-like carbon pore of  $H = 0.6$  nm at 77 K. The average gyration radius of ring polymer in the bulk phase is  $R_g = 0.29$  Å. The fluid-fluid interactions between the beads of hydrogen ring polymers were modeled by: solid lines – spherical 12-6 Lennard-Jones interaction potential, open circles – spherical Silvera-Goldman<sup>33</sup> effective intermolecular potential. The calculations were performed for:  $\epsilon_{sf}$ ,  $\epsilon_{sf}/2$ ,  $\epsilon_{sf}/10$ , and hard-walls.

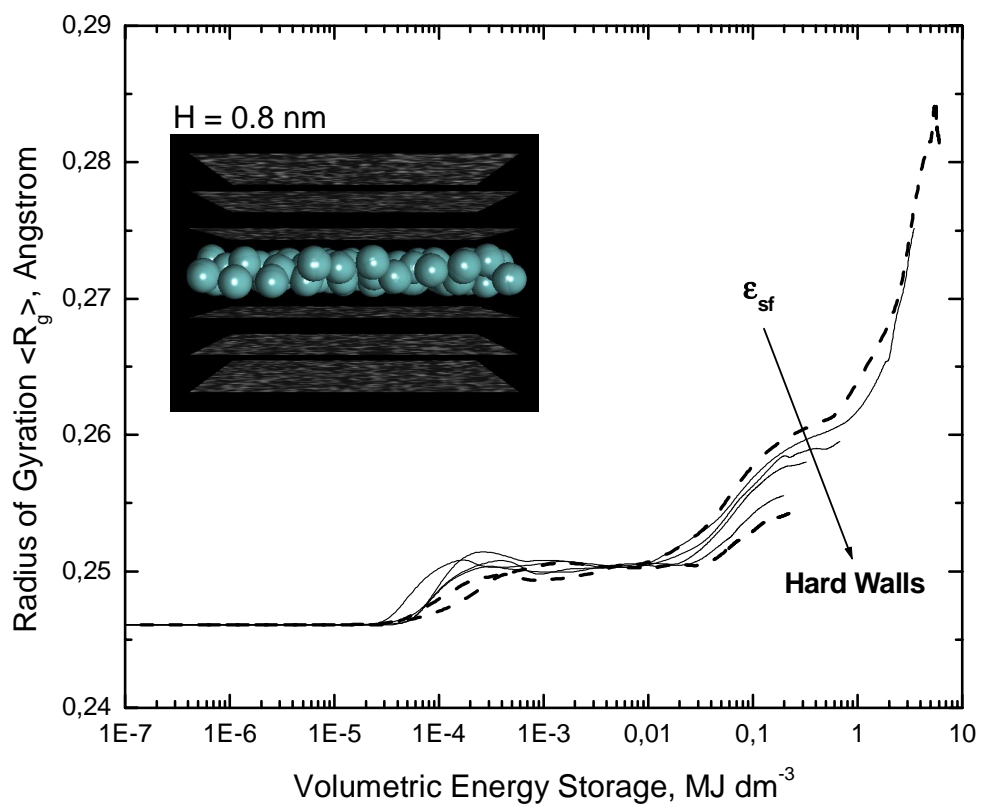


**Figure 3S.** Impact of the strength of  $\epsilon_{sf}$  on the average size of adsorbed hydrogen ring polymers in slit-like carbon pore of  $H = 0.8\text{ nm}$  at  $77\text{ K}$ . The average gyration radius of ring polymer in the bulk phase is  $R_g = 0.29\text{ \AA}$ . The calculations were performed for:  $\epsilon_{sf}$ ,  $\epsilon_{sf}/2$ ,  $\epsilon_{sf}/5$ ,  $\epsilon_{sf}/10$ ,  $\epsilon_{sf}/100$ ,  $\epsilon_{sf}/1000$ , and hard-walls.

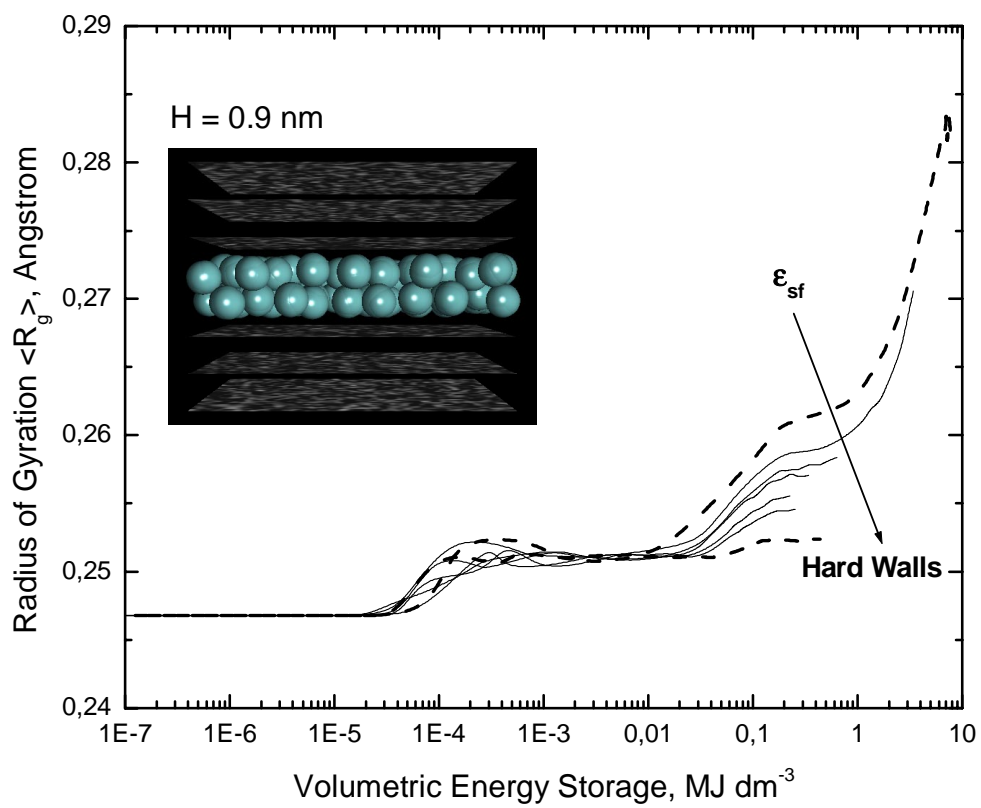


**Figure 4S.** Impact of the strength of  $\epsilon_{sf}$  on the average size of adsorbed hydrogen ring polymers in slit-like carbon pore of  $H = 0.9\text{ nm}$  at 77 K. The average gyration radius of ring polymer in the bulk phase is  $R_g = 0.29\text{ \AA}$ . The calculations were performed for:  $\epsilon_{sf}$ ,  $\epsilon_{sf}/2$ ,  $\epsilon_{sf}/5$ ,  $\epsilon_{sf}/10$ ,  $\epsilon_{sf}/100$ ,  $\epsilon_{sf}/1000$ , and hard-walls.

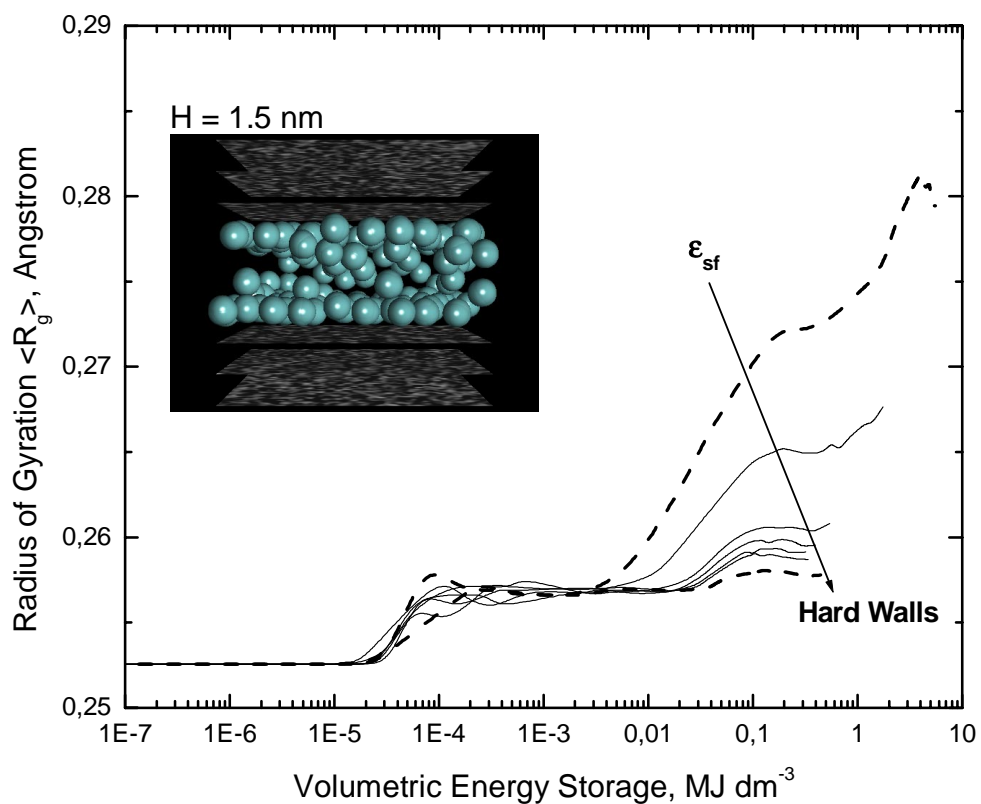


**Figure 5S.** Impact of the strength of  $\epsilon_{sf}$  on the average size of adsorbed hydrogen ring polymers in slit-like carbon pore of  $H = 1.5$  nm at 77 K. The average gyration radius of ring polymer in the bulk phase is  $R_g = 0.29$  Å. The calculations were performed for:  $\epsilon_{sf}$ ,  $\epsilon_{sf}/2$ ,  $\epsilon_{sf}/5$ ,  $\epsilon_{sf}/10$ ,  $\epsilon_{sf}/100$ ,  $\epsilon_{sf}/1000$ , and hard-walls.